

Growth of Antiperovskite Oxide Ca_3SnO Films by Pulsed Laser Deposition

Makoto Minohara^{1,2*}, Ryu Yukawa¹, Miho Kitamura¹, Reiji Kumai^{1,2}, Youichi Murakami^{1,2}
and Hiroshi Kumigashira^{1,2}

*Corresponding author Tel: +81 29 864 5586

E-mail: minohara@post.kek.jp

¹*Photon Factory, Institute of Materials Structure Science (IMSS), High Energy Accelerator Research Organization (KEK), Tsukuba, Ibaraki 305-0801, Japan*

²*Department of Materials Structure Science, SOKENDAI (The Graduate University for Advanced Studies), Tsukuba, Ibaraki 305-0801, Japan*

Abstract

We report the epitaxial growth of Ca_3SnO antiperovskite oxide films on (001)-oriented cubic yttria-stabilized zirconia (YSZ) substrates by using a conventional pulsed laser deposition (PLD) technique. In this work, a sintered Ca_3SnO pellet is used as the ablation target. X-ray diffraction measurements demonstrate the (001) growth of Ca_3SnO films with the antiperovskite structure and a cube-on-cube orientation relationship to the YSZ substrate. The successful synthesis of the antiperovskite phase is further

confirmed by x-ray photoemission spectroscopy. These results strongly suggest that antiperovskite-oxide films can be directly grown on substrates from the target material using a PLD technique.

Keywords

A3. Pulsed laser deposition

B1. Antiperovskite oxides

Main text

1. Introduction

Perovskite oxides are an important class of materials that exhibit novel functional properties [1]. Recently, their counterpart materials, namely antiperovskite oxides A_3BO ($A = \text{Ca, Sr, Ba}$; $B = \text{Sn, Pb}$), have been attracting attention as an alternative platform for prospecting unique physical properties. Following the theoretical prediction that some materials in the antiperovskite-oxide family have three-dimensional Dirac fermions [2], a number of experimental and theoretical efforts have been devoted to exploring the possible presence of bulk Dirac fermions in antiperovskite oxides [3-8]. Since this unique electronic structure is predicted to appear in the bulk and not at the surface, heterostructures composed of perovskite and antiperovskite oxides might also be promising candidates for exploratory studies of novel physical properties, analogous to the studies of perovskite oxide heterostructures [9-13]. Despite these intriguing research opportunities, there are few reports on the growth of antiperovskite-oxide films [7,8].

Since the pulsed laser deposition (PLD) technique is capable of growing films from a wide variety of materials, this technique is well-suited for the rapid investigation of antiperovskite-oxide films. However, since the use of PLD for the growth of these films is still in its infancy, whether antiperovskite-oxide films can be really grown by PLD remains to be convincingly answered. X-ray diffraction (XRD) measurements from the reported antiperovskite-oxide films grown by an “unconventional” PLD technique, where the films were grown by alternating deposition of AO and BO_2 targets, did not show any of the characteristic Bragg reflections from $(00l)$ planes with an odd l that should be expected for an antiperovskite phase [7]. Therefore, the development of reliable methods for the growth of antiperovskite-oxide films by PLD is necessary, not only for exploring novel functionalities, but also for elucidating unique band structures via spectroscopic measurements [14-16].

In this study, we report the conventional PLD growth of an antiperovskite-oxide Ca_3SnO film by using the antiperovskite-oxide ceramic target as the source material. By varying the substrate temperature ($T_{sub.}$) and the oxygen partial pressure (P_{O_2}) during growth, we identify the optimum growth condition for Ca_3SnO thin films. XRD results indicate the formation of the antiperovskite structure and its cube-on-cube epitaxial relationship to the substrate. The successful growth of antiperovskite phase is further confirmed by x-ray photoemission spectroscopy (XPS): The shape of the valence band spectrum is qualitatively reproduced by the first-principles calculation for Ca_3SnO .

2. Experimental Section

Ca_3SnO films were grown on (001)-oriented yttria-stabilized zirconia (YSZ) single-crystal substrates in a vacuum chamber by a PLD technique using a sintered

Ca₃SnO target. A Nd-doped yttrium aluminum garnet laser was used for ablation in its frequency-tripled mode ($\lambda = 355$ nm) at a repetition rate of 1 Hz. Prior to film deposition, YSZ substrates were annealed in air, in an electric furnace at 1400 °C, to obtain an atomically flat surface. To optimize the growth conditions, T_{sub} and P_{O_2} were varied under a fixed laser fluence of ~ 4.6 mJ/cm². The surface crystalline quality during growth was monitored *in situ* by reflective high-energy electron diffraction (RHEED).

The epitaxial relationship and crystalline quality were analyzed using *ex situ* synchrotron-based XRD, which was carried out at beamline 7C in the Photon Factory, KEK. The energy of the incident x-ray was 9 keV. For XRD measurements, Au was deposited as a capping layer to prevent degradation by moisture in the air. XPS measurements were performed using a VG-Scienta R3000 electron energy analyzer with a monochromatized Al $K\alpha$ x-ray source ($h\nu = 1486.6$ eV). For XPS measurements, the samples were transported to an analysis chamber without air exposure using a home-built vacuum suitcase. Binding energies were calibrated by measuring a gold film, electrically connected to the samples. All spectra were acquired at room temperature with a total energy resolution of 500 meV.

First-principles calculations based on density-functional theory were carried out in the framework of the Perdew-Burke-Ernzerhof-type generalized-gradient approximation [17] using the WIEN2k code [18], where spin-orbit interactions are taken into account. An idealized cubic structure was assumed with the empirical lattice constant of $a = 4.83$ Å [19]. The corresponding Brillouin zone was sampled by $20 \times 20 \times 20$ momentum points.

3. Results and discussion

3.1 Optimization of the growth conditions for Ca₃SnO films

In general, the guidance of Ellingham diagrams, in which the stable valence states of simple metal oxides are mapped in terms of standard-state Gibbs free energy and temperature, is useful in deducing optimal growth conditions. However, since Ca₃SnO exhibits an unusual Sn valence state of Sn⁴⁺, it is difficult to identify the processing “sweet spot” using the Ellingham diagram, as there are no thermodynamic data available for Sn⁴⁺ [20,21]. Therefore, we optimize Ca₃SnO thin film growth by varying $T_{\text{sub.}}$ and P_{O_2} over a rather wide range of values. Figure 1(a) shows the RHEED patterns for the thin films grown at various $T_{\text{sub.}}$ and P_{O_2} . There are two discrete regions showing the clear streak patterns indicative of the epitaxial growth of certain oxides; A region at $T_{\text{sub.}} = 900$ °C without oxygen flow and another between $T_{\text{sub.}} = 700$ and 750 °C under a P_{O_2} of 10^{-6} to 10^{-7} Torr. Since the RHEED pattern changes in a discontinuous manner, we surmise that different oxides are grown under these two discrete conditions. In order to survey the chemical composition of these thin films, we performed auger electron spectroscopy (AES). Figure 1(b) shows AES results for samples α ($T_{\text{sub.}} = 900$ °C, without oxygen flow) and β ($T_{\text{sub.}} = 700$ °C, $P_{\text{O}_2} = 10^{-7}$ Torr), representative of the above-mentioned regions [also see Fig. 1(a)]. The AES results reveal the difference between these samples. While sample α does not contain Sn ions, sample β does. The disappearance of Sn for the sample α may originate from the high volatility of Sn and its oxides (SnO and SnO₂) [22] at $T_{\text{sub.}} = 900$ °C, strongly suggesting that only the growth of the remnant CaO_{*x*} is stabilized at this higher temperature region. From these results, the optimum conditions for Ca₃SnO growth could be in the range of $T_{\text{sub.}} = 700$ to 750 °C under a P_{O_2} of 10^{-6} to 10^{-7} Torr.

3.2 Structural analysis

We performed XRD measurements to verify the formation of antiperovskite Ca_3SnO . Figure 2(a) shows the out-of-plane XRD 2θ - θ pattern for the sample β . Some characteristic peaks are clearly observed. In order to index these peaks, we compare the measured 2θ - θ XRD pattern with the calculated patterns of Ca_3SnO (antiperovskite structure), CaSnO_3 (perovskite structure), and CaO (rocksalt structure), since CaSnO_3 and CaO are also potentially synthesized under such an oxidizing atmosphere [20-22]. The calculated $(00l)$ Bragg peaks of the three potential oxides are shown in the Fig. 2(b). Comparison of the measured XRD pattern with the calculated patterns shows that the observed peaks in Fig. 2(a) correspond to the characteristic $(00l)$ Bragg peaks of Ca_3SnO . Since rocksalt CaO and Ca_3SnO have near identical lattice constants, a $(00l)$ peak with an odd l is key to distinguishing these two structures. Since a (001) peak is observed, the XRD results provide strong evidence for the formation of antiperovskite Ca_3SnO films by PLD under the identified optimum conditions, although the existence of some impurity phases is surveyed. Considering both the formation energy in the materials project database [23] and the calculated peak positions of candidate materials comprised of Ca, Sn and O atoms [23], the impurity phases might be $\text{Ca}_2\text{Sn}_3\text{O}_8$ or Ca_2SnO_4 . Although the precise identification of the impurity phase is difficult at the moment, the existence of the impurity phase implies an off-stoichiometry composition in the Ca_3SnO film. Indeed, the intensity ratio of (001) to (002) Bragg peaks is evaluated to be 0.18, which is slightly smaller than the ideal ratio of 0.27, suggesting the presence of structural disorder in the Ca_3SnO films owing to the existence of impurity phases and a possible off-stoichiometry composition [8].

Next, we investigate the crystalline quality of Ca_3SnO films and its epitaxial relationship with YSZ (001) substrate. As shown in Fig. 2(c), the full-width at half-maximum of the rocking curve for the (002) diffraction is evaluated to be around 0.14° . This value is one order of magnitude narrower than that of Sr_3SnO antiperovskite films grown by molecular beam epitaxy [8]. This result identifies the current PLD-grown films as being highly crystalline, despite the impurity phases observed in the 2θ - θ pattern. Figure 2(d) shows the *phi*-scan of XRD patterns on {202} reflections for Ca_3SnO films, together with that of YSZ substrates with cubic symmetry. The peaks are clearly observed every 90° for the film as well as the substrate, reflecting the four-fold symmetry of antiperovskite structure. This result indicates the cube-on-cube epitaxial relationship between the YSZ (001) substrate and the Ca_3SnO film.

3.3 Chemical state analysis

In order to analyze the chemical state of constituent elements, XPS measurements were performed on the Ca_3SnO film (sample β). The XPS spectra for Sn- $3d$, Ca- $2p$, and O- $1s$ core levels are shown in Figs. 3(a), (b), and (c), respectively, along with the results of peak deconvolution by curve-fitting analysis. Since the intensity of the peaks at higher binding energies became stronger with increasing photoelectron emission angle (not shown), the higher (lower) peaks can be assigned to the surface (bulk) components for all core levels. For the Sn- $3d$ core level, the bulk and surface components for Sn $3d_{5/2}$ states are evaluated to be positioned at energies of ~ 484.8 eV and ~ 486.7 eV, respectively. In terms of chemical shift, the surface component can be assigned to either Sn^{4+} (486.0–487.3 eV) or Sn^{2+} (485.6–487 eV) [24], suggesting the

segregation of Sn oxides (SnO₂ or SnO, respectively) to the surface of the Ca₃SnO films.

On the other hand, the peak position of the bulk component is unusual in oxides: The energy of ~484.8 eV for Sn 3d_{5/2} states is close to that of Sn metal or its intermetallic alloys (Sn⁰: 484.3–485.2 eV) [24]. The unusual chemical shift of Sn ions might imply the existence of possible Sn⁴⁺ states in Ca₃SnO as following reasons, although the chemical shift of Sn⁴⁺ is not known yet. Assuming that the Sn ions in Ca₃SnO are close to Sn⁰ states (antiperovskite Ca₃SnO is an intermetallic), the Ca ions should be also close to Ca⁰. However, as shown in Fig. 3(b), the peak position of the bulk Ca 2p_{3/2} states (346.8 eV) is significantly different from that of Ca metal and its alloys (344.9–346.0 eV) [24]. Based on the chemical shifts of Ca²⁺ states (346.1–347.3 eV) [24], the valence of Ca ions in the Ca₃SnO film is assigned to Ca²⁺. Moreover, the chemical shift of the O-1s core level can be also ascribed to O²⁻ as shown in Fig. 3(c) [24]. From these experimental results, it could be reasoned that Sn ions in Ca₃SnO are close to an unusual valence state of Sn⁴⁺, although further theoretical investigation is necessary to clarify such an unusual the chemical states of Sn ions in Ca₃SnO.

3.4 Analysis of electronic structure

The successful synthesis of the antiperovskite phase of Ca₃SnO is further supported by valence band (VB) spectra shown in Fig. 4. The upper panel of Fig. 4 shows the VB spectrum of Ca₃SnO film (sample β), together with the density of states (DOS) obtained by the first-principles calculations. The reported XPS spectra of CaO [25], CaSnO₃ [26], SnO₂ [27], SnO [27], and Sn metal [28] are shown in the lower panel of Fig. 4 as references. Overall, the VB spectrum of Ca₃SnO film is significantly different from those of the referenced materials. The characteristic feature in the Ca₃SnO spectrum

is the existence of a band in the energy range between the Fermi level and ~ 3 eV. This feature of the VB spectra is approximately captured by the first-principles calculation for Ca_3SnO , although there are some discrepancies in the peak positions for bands located at higher binding energies (upper panel, Fig. 4). Therefore, the XPS results provides additional confirmation of the formation of Ca_3SnO .

4. Conclusions

We have demonstrated that the antiperovskite oxide Ca_3SnO film can be grown on a YSZ (001) substrate by using a Ca_3SnO target in a conventional pulsed laser deposition (PLD) technique. By varying the temperature of the substrate and the partial pressure of oxygen during growth, we identified the optimal conditions for the PLD growth of Ca_3SnO films. The successful growth of epitaxial Ca_3SnO films on YSZ substrates is confirmed by x-ray diffraction measurements. The *phi*-scan of {202} reflections reveals the cube-on-cube epitaxial relationship between the Ca_3SnO film and the YSZ (001) substrate. The synthesis of the antiperovskite phase of Ca_3SnO is further supported by x-ray photoemission spectroscopy. The results show that antiperovskite-oxide films can be directly synthesized from the target by using a PLD technique just like several other widely-studied oxide films. The present demonstration of the growth of antiperovskite oxides by PLD might be a promising avenue for the research of antiperovskite oxides in film form as well as artificial antiperovskite/perovskite oxide structures.

Acknowledgments

We thank Hironori Nakao for useful discussions. This work was supported by a

Grant-in-Aid for Scientific Research (No. B25287095 and 16H02115) and a Grant-in-Aid for Young Scientists (No. 15K17470) from the Japan Society for the Promotion of Science (JSPS) as well as the MEXT Elements Strategy Initiative to Form Core Research Center. The work at KEK-PF was performed under the approval of the Program Advisory Committee (Proposals No. 2013S2-002 and 2015S2-005) at the Institute of Materials Structure Science, KEK.

References

- 1) H. Y. Hwang, Y. Iwasa, M. Kawasaki, B. Keimer, N. Nagaosa, and Y. Tokura, *Nat. Mater.* **11**, 103 (2012).
- 2) T. Kariyado, and M. Ogata, *J. Phys. Soc. Jpn.* **80**, 083704 (2011).
- 3) M. Klintonberg, J. T. Haraldsen, and A. V. Balatsky, *Appl. Phys. Res.* **6**, 31 (2014).
- 4) T. H. Hsieh, J. Liu, and L. Fu, *Phys. Rev. B* **90**, 081112 (2014).
- 5) M. Oudah, A. Ikeda, J. N. Hausmann, S. Yonezawa, T. Fukumoto, S. Kobayashi, M. Sato, and Y. Maeno, *Nat. Commun.* **7**, 13617 (2016).
- 6) Y. Okamoto, A. Sakamaki, and K. Takenaka, *J. Appl. Phys.* **119**, 205106 (2016).
- 7) Y. F. Lee, F. Wu, R. Kumar, F. Hunte, J. Schwartz, and J. Narayan, *Appl. Phys. Lett.* **103**, 112101 (2013).
- 8) D. Samal, H. Nakamura, and H. Takagi, *APL Mater.* **4**, 076101 (2016).
- 9) A. Ohtomo, and H. Y. Hwang, *Nature* **427**, 423 (2004).
- 10) N. Reyren, S. Thiel, A. D. Caviglia, L. F. Kourkoutis, G. Hammerl, C. Richter, C. W. Schneider, T. Kopp, A. S. Ruetschi, D. Jaccard, M. Gabay, D. A. Muller, J. M. Triscone, and J. Mannhart, *Science* **317**, 1196 (2007).
- 11) K. S. Takahashi, M. Kawasaki, and Y. Tokura, *Appl. Phys. Lett.* **79**, 1324 (2001).
- 12) T. Koida, M. Lippmaa, T. Fukumura, K. Itaka, Y. Matsumoto, M. Kawasaki, and H. Koinuma, *Phys. Rev. B* **66**, 144418 (2002).
- 13) S. J. May, A. B. Shah, S. G. E. te Velthuis, M. R. Fitzsimmons, J. M. Zuo, X. Zhai, J. N. Eckstein, S. D. Bader, and A. Bhattacharya, *Phys. Rev. B* **77**, 174409 (2008).
- 14) T. Ohta, A. Bistwick, J. L. McChesney, T. Seyller, K. Horn, and E. Rotenberg, *Phys. Rev. Lett.* **98**, 206802 (2007).
- 15) D. Hsieh, D. Qian, L. Wray, Y. Xia, Y. S. Hor, R. J. Cava, and M. Z. Hasan, *Nature* **452**,

970 (2008).

- 16) S.-Y. Xu, N. Alidoust, I. Belopolski, Z. Yuan, G. Bian, T.-R. Chang, H. Zheng, V. N. Strocov, D. S. Sanchez, G. Chang, C. Zhang, D. Mou, Y. Wu, L. Huand, C.-C. Lee, S.-M. Huang, B. K. Wang, A. Bansil, H.-T. Jeng, T. Neupert, A. Kaminski, H. Lin, S. Jia, and M. Z. Hasan, *Nat. Phys.* **11**, 748 (2015).
- 17) J. P. Perdew, K. Burke, and M. Ernzerhof, *Phys. Rev. Lett.* **77**, 3865 (1996).
- 18) P. Blaha, K. Schwarz, G. K. H. Madsen, D. Kvasnicka, and J. Luitz: *WIEN2k, An Augmented Plane Wave + Local Orbitals Program for Calculating Crystal Properties* (Karlheinz Schwarz, Techn. Universität Wien, Austria, 2001) ISBN 3-9501031-1-2.
- 19) A. Widera and H. Schäfer, *Mater. Res. Bull.* **15**, 1805 (1980).
- 20) *CRC Handbook of Chemistry and Physics*, 61st ed.; Weast, R. C., Astle, M. J., Eds.; CRC Press: Boca Raton, FL, 1980; pp D67-77.
- 21) *NIST Chemistry WebBook, NIST Standard Reference Database Number 69*, edited by P. J. Linstrom and W. G. Mallard. <http://webbook.nist.gov/chemistry/>.
- 22) I. Barin, O. Knacke, and O. Kubaschewski, In *Thermochemical Properties of Inorganic Substances* (Springer, 1977).
- 23) A. Jain, S. P. Ong, G. Hautier, W. Chen, W. D. Richards, S. Dacek, S. Cholia, D. Gunter, D. Skinner, G. Ceder, and K. A. Persson, *APL Mater.* **1**, 011002 (2013).
- 24) *NIST X-ray Photoelectron Spectroscopy Database, NIST Standard Reference Database Number 20*, edited by A. V. Naumkin, A. Kraut-Vass, S. W. Gaarenstroom, and C. J. Powell. <https://srdata.nist.gov/xps/>.
- 25) D. Ochs, B. Braun, W. Maus-Friedrichs, and V. Kempter, *Surf. Sci.* **417**, 406 (1998).
- 26) J. D. Baniecki, T. Yamazaki, D. Ricinschi, Q. V. Overmeere, H. Aso, Y. Miyata, H. Yamara, N. Fujimura, R. Maran, T. Anazawa, N. Valanoor, and Y. Imanaka, *Sci. Rep.* **7**,

41725 (2017).

27) Y. Ogo, H. Hiramatsu, K. Nomura, H. Yanagi, T. Kamiya, M. Kimura, M. Hirano, and H. Hosono, *Phys. Status Solidi A* **206**, 2187 (2009).

28) H. Höchst, S. Hüfner, and A. Goldman, *Solid State Commun.* **19**, 899 (1976).

Figure Captions

Fig. 1 (Color online) (a) A map of RHEED patterns from thin films grown on a YSZ (001) substrate at various $T_{\text{sub.}}$ and P_{O_2} . (b) Auger electron spectra of thin films labeled α and β that are grown at $T_{\text{sub.}} = 900$ °C with no oxygen flow (red) and $T_{\text{sub.}} = 700$ °C with $P_{\text{O}_2} = 10^{-7}$ Torr (blue), respectively.

Fig. 2 (Color online) (a) The 2θ - θ XRD pattern of sample β . The asterisks indicate the peaks from a capped gold film, while the diamonds are from impurities. (b) Calculated XRD patterns for Ca_3SnO , CaSnO_3 , and CaO . The bars correspond to $(00l)$ peaks. (c) The rocking curve for the (002) Bragg reflection of grown films. (d) ϕ -scans for $\{202\}$ reflection of the YSZ substrate (upper panel) and grown thin film (lower panel).

Fig. 3 (Color online) XPS spectra from the Ca_3SnO film (sample β) for (a) Sn-3d, (b) Ca-2p, and (c) O-1s core levels. The fitting results are overlaid by green, blue, and red curves, which correspond to the surface component (S), bulk component (B), and their summation, respectively.

Fig. 4 (Color online) (upper panel) The valence band spectrum of a Ca_3SnO film (sample β), together with the DOS obtained from the first principle calculation. In order to emphasize the gap-like feature in the Ca_3SnO film near the Fermi level (E_{F}) of the sample, the Fermi edge of gold film is superimposed. (Lower panel) The reference spectra of CaO [25], CaSnO_3 [26], SnO_2 [27], SnO [27], and Sn metal [28].

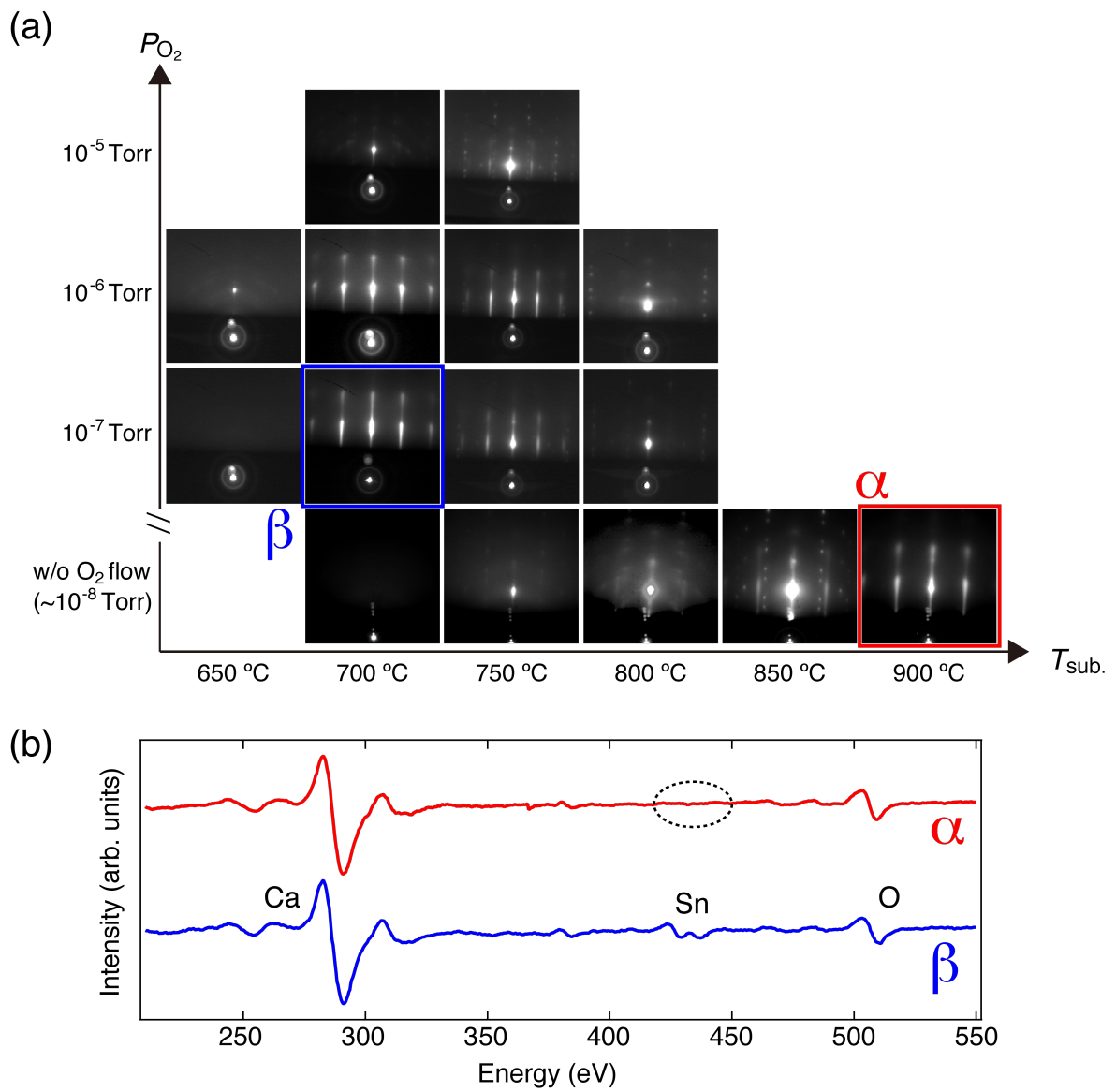


Fig. 1. (Color Online)

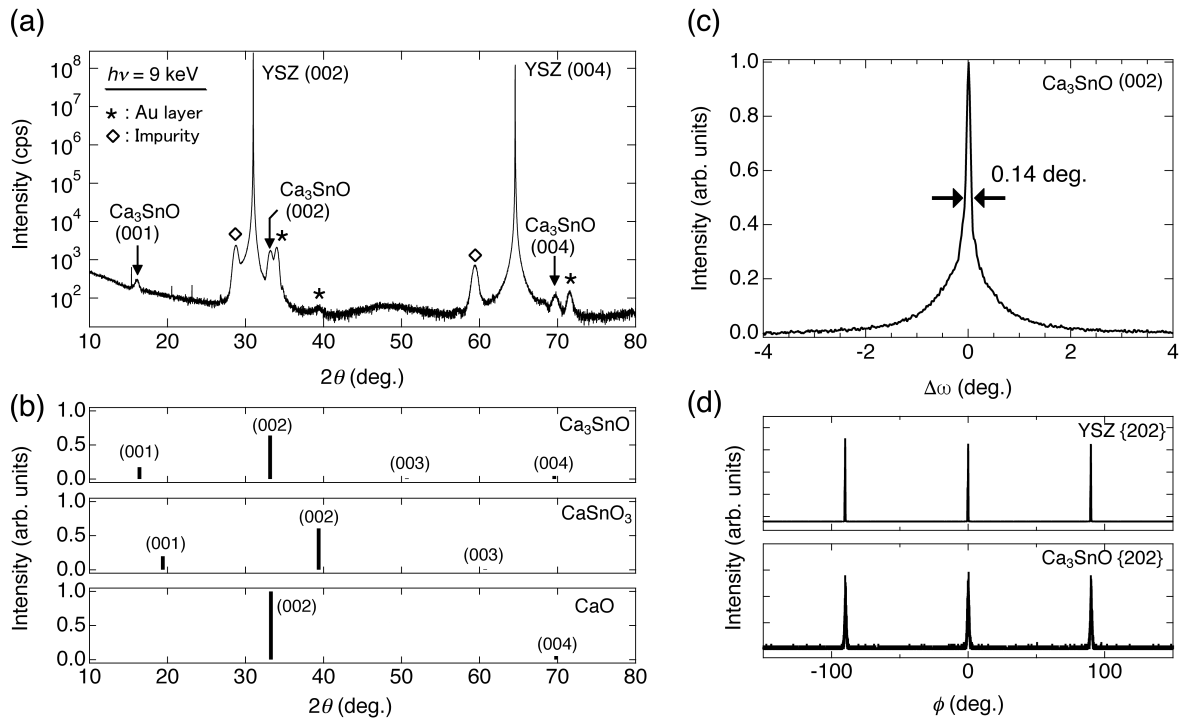


Fig. 2. (Color Online)

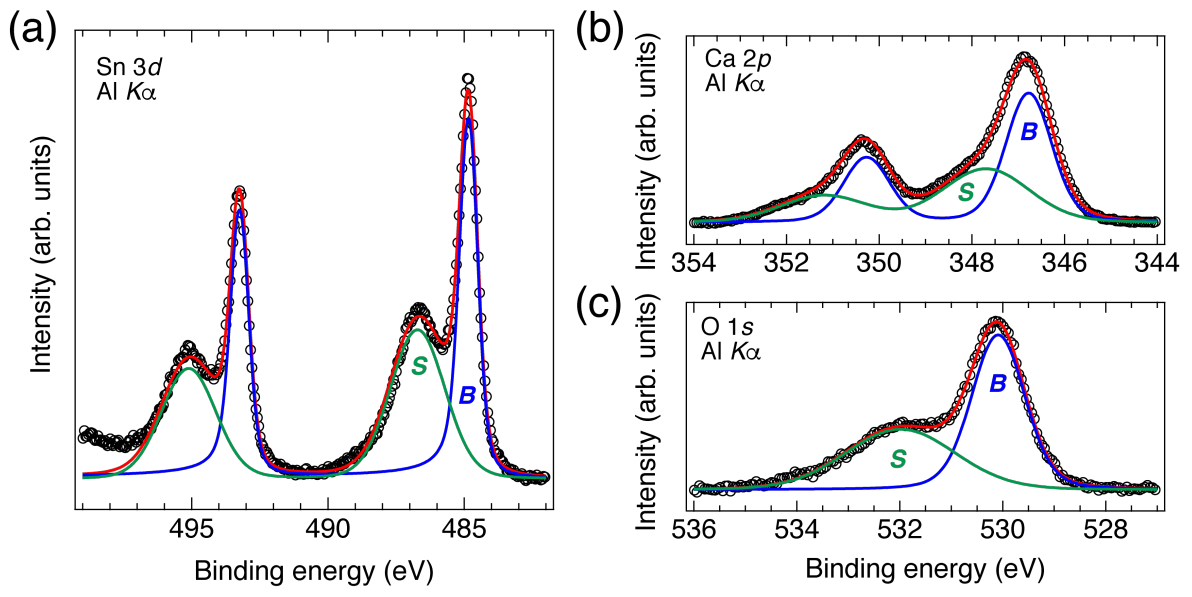


Fig. 3. (Color Online)

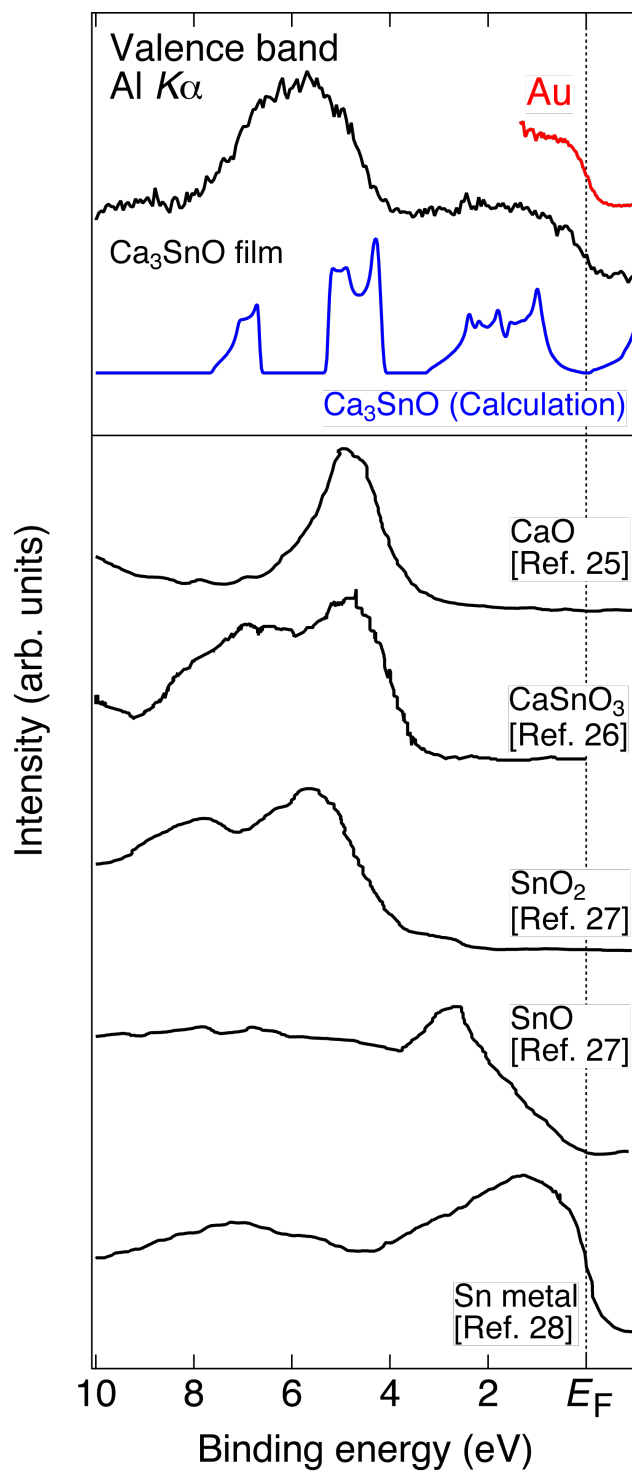


Fig. 4. (Color Online)